Journal of the Mechanical Behavior of Biomedical Materials 101 (2020) 103416

Contents lists available at ScienceDirect

Journal of the Mechanical Behavior of Biomedical Materials

journal homepage: www.elsevier.com/locate/jmbbm

Bone regeneration into side openings and hollow inner channel of a dental implant

Do-Gyoon Kim[a,*], Kyoung-Hwa Kim[b], YeHyeon Jo[c], Jue Yeon Lee[d], Yoon Jeong Park[e], Chong Pyoung Chung[d], Yang-Jo Seol[b,**], Jung-Suk Han[c,***]

[a] Division of Orthodontics, College of Dentistry, The Ohio State University, Columbus, OH, 43210, USA
[b] Department of Periodontology and Dental Research Institute, School of Dentistry, Seoul National University, Jongno, Seoul, 03080, South Korea
[c] Department of Prosthodontics and Dental Research Institute, School of Dentistry, Seoul National University, Seoul, South Korea
[d] Central Research Institute, Nano Intelligent Biomedical Engineering Corporation (NIBEC), Seoul, 03080, South Korea
[e] Department of Dental Regenerative Bioengineering and Dental Research Institute, School of Dentistry, Seoul National University, Seoul, 03080, South Korea

ARTICLE INFO

Keywords:
Dental implant
Bone regeneration
Nanoindentation

ABSTRACT

The current study examined whether bone can regenerate into an open space fabricated inside the metal implant and maintain its quantity and quality at the early post-implantation healing periods. 12 conventional one piece screw type titanium dental implants (control group) and 12 hybrid dental implants with spiral side openings (0.58 mm wide) connected to hollow inner channel (experimental group) were bilaterally placed in each quadrant at the P3, P4 and M1 positions in mandible of 4 adult beagles following 2 months of post-extraction healing. Fluorescent bone labels to qualitatively evaluate newly formed bone tissues were administered at 2 and 4 weeks of post-implantation periods, respectively. 3 control and 3 experimental bone-implant constructs for each animal were dissected from 2 animals at each 3 and 6 weeks of post-implantation healing periods. Undecalcified specimens were prepared from each construct for histological analyses to measure bone-to-implant contact (BIC) and interfacial bone area (BA), and also for nanoindentation and scanning electron microscopy to assess elastic modulus (E) and composition of bone tissues surrounding the implants, respectively. A substantial amount of newly formed bone tissues were observed at the implant interfaces of both implant groups. Bone tissues successfully regenerate through the side openings and hollow inner channel of the experimental implant as early as 3 weeks of post-implantation healing. The E values of the newly formed bone tissues were measured comparable to those of normal bone tissues. The current results indicate that the new hybrid implant can conduct bone regeneration into the inner architecture, which likely improves stability of the implant system by enhancing integrity of implant with interfacial bone.

1. Introduction

Dental implant surgery has a success rate higher than 94%, leading to more than a million dental implantations annually and a continually increasing number of clinical cases (Charyeva et al., 2012; Pjetursson et al., 2014; Greenstein and Cavallaro, 2014). This high success rate is guaranteed only when the quantity and quality of bone at the surgical site are conducive to the implant placement. However, most patients who need dental implantation have various levels of bone deficiency due to oral bone complications that cause the initial extraction of teeth and bone loss following the extraction (Greenstein and Cavallaro, 2014; Tonetti et al., 2008). For example, tooth extraction and disuse atrophy arising from delayed treatment can lead to loss of the alveolar ridge (Wang and Lang, 2012; Horowitz et al., 2012). As such, there is an increasing demand for a new dental implant system that can maintain its stability while minimizing influences from bone quantity and quality surrounding the implant.

Osseointegration delineates a direct bone apposition on the implant surface without getting soft tissue (Brunski, 1988; Branemark et al., 1977; Bosshardt et al., 2017). In addition to the osseointegration on the

* Corresponding author. Division of Orthodontics, College of Dentistry, The Ohio State University, 4088 Postle Hall, 305 W. 12th Ave, Columbus, OH, 43210, USA.
** Corresponding author. Department of Periodontology and Dental Research Institute, School of Dentistry, Seoul National University, 62 Changgyeonggungno, Jongno-Gu, Seoul, 110-749, South Korea.
*** Corresponding author. Department of Prosthodontics, School of Dentistry, Seoul National University, 62 Changgyeonggungno, Jongno-Gu, Seoul, 110-749, South Korea.
E-mail addresses: kim.2508@osu.edu (D.-G. Kim), yjseol@snu.ac.kr (Y.-J. Seol), proshan@snu.ac.kr (J.-S. Han).

https://doi.org/10.1016/j.jmbbm.2019.103416
Received 28 March 2019; Received in revised form 30 August 2019; Accepted 2 September 2019
Available online 03 September 2019
1751-6161/

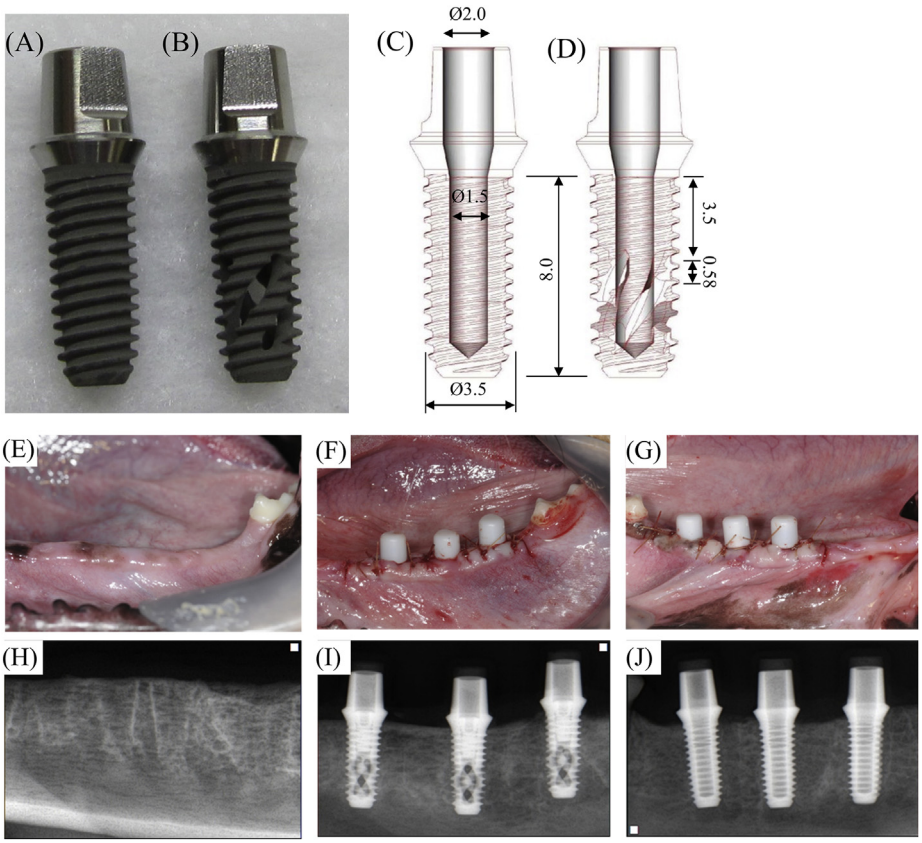

Fig. 1. (A) Conventional one piece titanium dental implants (control group) and (B) one piece hybrid dental implants having spiral side openings (experimental group), (C) engineering drawings for each implant design, (D) the spiral side openings connected to the hollow inner channel (unit: mm). Clinical photographs (upper panel) and radiographs (lower panel) of implantation procedure. (E), (H) Extraction sites after 8 weeks of the post-implantation healing period. (F), (I) Experimental implants, (G), (J) Control implants.

implant surface, bone ingrowth into a hollow dental implant was introduced, which was expected to enhance stability of the implant system (Scacchi, 2000). It was observed that bone grew into the transverse holes on the cylindrical side walls and inner hollow basket body (Piattelli et al., 1999; Takeshita et al., 1996). The long-term survival rate of this hollow dental implant system was higher than 85 % (Telleman et al., 2006; Karoussis et al., 2004). However, this hollow implant system was limited with potential risks of less stable structure for load-bearing due to the side holes and cylindrical hollow bucket with open bottom floor of the implant body (Behneke et al., 2002; Hellem et al., 2001; Buser et al., 1997).

Recently, we have developed a new dental implant that has spiral side openings connected to hollow inner channel and top opening (Fig. 1). This hybrid implant is fabricated with upper thread portion, side openings onto the threads at the middle portion, and closed bottom with lower thread portion. We hypothesize that this hybrid architecture of threads with openings may successfully conduct bone ingrowth into the open inner space while maintaining and enhancing the mechanical stability of the dental implant system. Thus, the objective of the current study was to examine whether bone can regenerate into an open space fabricated inside the metal implant and maintain its quantity and quality at the early post-implantation healing periods.

2. Materials and methods

2.1. Animal model

Four adult male beagles weighing 10–12 kg (12 months of age) were used in this study. All of the animals had fully erupted permanent dentition. The animal research protocol was approved by the Institute of Laboratory Animal Resources, Seoul National University (SNU-170417-13).

2.2. Dental implants

Conventional one piece titanium dental implants (3.5 mm in diameter and 8 mm in length) with a hollow inner channel and large grit sandblast and acid-etched (SLA) surface (Shinhung, Seoul, Korea) were prepared as the control group for animal experiments (Fig. 1A,C). Then, hybrid dental implants were fabricated by modifying the conventional dental implant to have spiral side openings connected to the hollow inner channel as the experiment group (Fig. 1B,D). The dimension (0.58 mm wide) of spiral side opening was determined by referring to a previous study that perform *in vivo* bone ingrowth to titanium porous scaffold implants with average pore sizes of 0.309, 0.632, and 0.956 mm (Taniguchi et al., 2016). As a result, the previous study observed that implant with the pore size of 0.632 mm showed the best mechanical strength, high fixation ability, and rapid bone ingrowth as early as 2 weeks following implantation. Many other studies used porous metal implants with average pore sizes between 0.5 mm and 0.7 mm also showed substantial *in vivo* bone ingrowth to the porous structure (Wang et al., 2017; Shah et al., 2016).

2.3. Surgical procedure

The animals were placed under general anesthesia and the surgical sites were locally anesthetized using 2% lidocaine hydrochloride with 1:100,000 epinephrine (Lignospan, France). All of the mandibular premolars and first molars (P1-M1) were bilaterally extracted (Fig. 1E,H). After 2 months of post-extraction healing, the dental implants were bilaterally placed in each quadrant at the P3, P4 and M1 positions of mandible according split-mouth design (Fig. 1F,G,I,J).Following implantation, an abutment screw was placed through top opening connected to the hollow inner channel of each implant. Then, a specially designed plastic healing cap was used to cover the abutment part of the one piece dental implant, which exposes above the gingival soft tissue. Fluorescent bone labels were used to

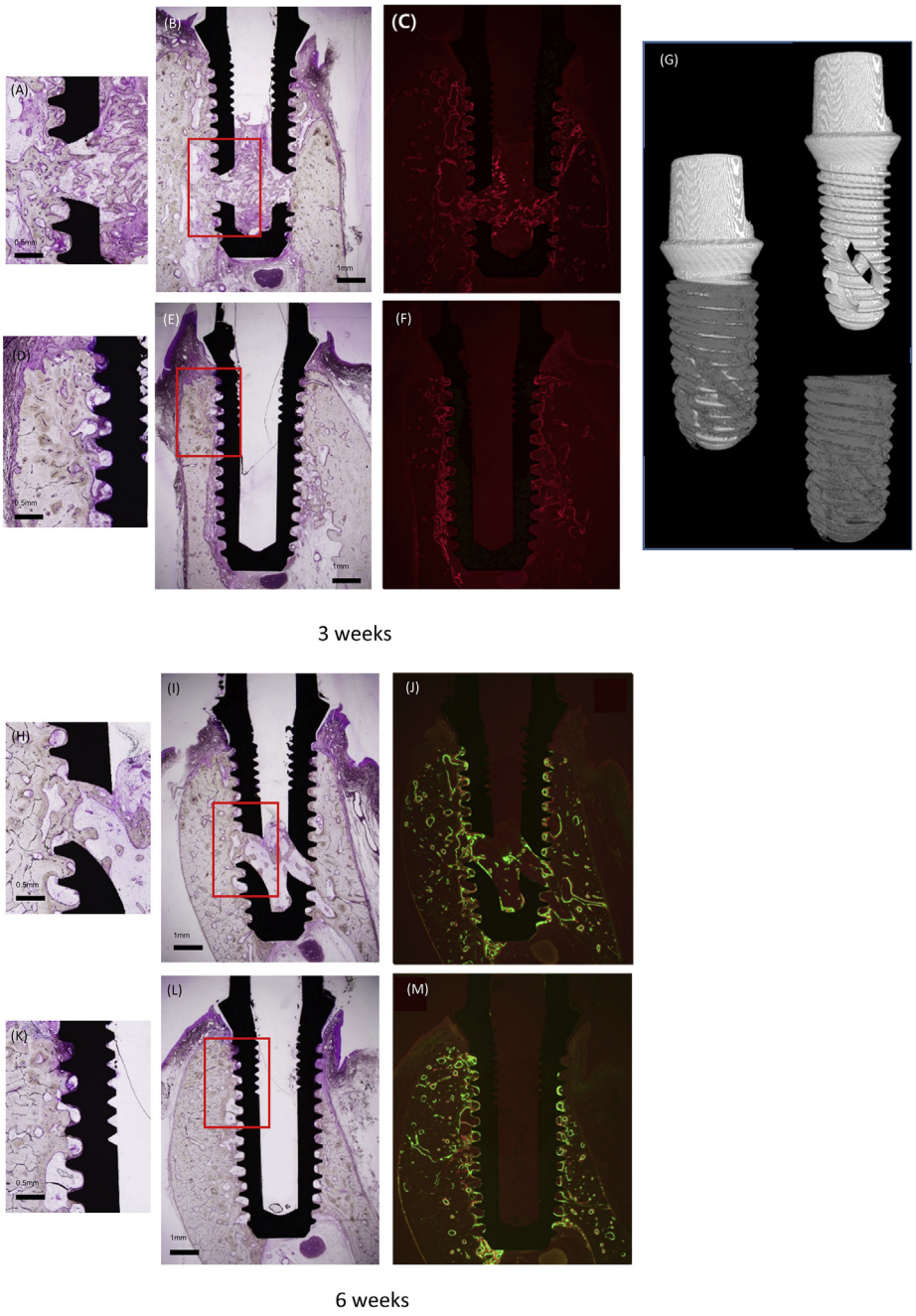

Fig. 2. Histology of the implant system at 3 weeks and 6 weeks of post-implantation healing for (A) (B) (H) (I)experimental implant group and (D) (E) (K) (L) control implant group. (A) (D) (H) (K) are the magnified regions of the red framed areas in (B) (E) (I) (L), respectively. (C) (F) (J) (M) are the fluorescent images for newly formed bone tissues labelled with Xylenol orange (red) at 2 weeks and Calcein (green) at 4 weeks after implantation. (G) 3D micro-CT image of the regenerated bone tissues in 300 μm surrounding the experimental implant at week 3. The implant and bone are digitally separated.

qualitatively evaluate new bone formation and remodeling adjacent implants. Xylenol orange (Sigma, St. Louis, MO) and calcein green (Sigma, St. Louis, MO) were administered at 2 and 4 weeks of post-implantation periods, respectively (Fig. 2). Two animals were sacrificed at 3 weeks and the other two animals were sacrifice at 6 weeks after implantation.

2.4. Micro-computed tomography (micro-CT)

The mandibles were block-resected in hydration using diamond saw (EXAKT, Norderstedt, Germany). The mandibular blocks were fixed in 10% neutralized buffered formalin and dehydrated using a series of ethanol solutions with increasing concentrations. Then, the blocks were embedded in resin media and scanned by a micro-CT (SkyScan1172-D, Kontich, Belgium) with 16 × 16 × 16 μm^3 voxel size under an identical scanning condition of 100 kV, 100 μA, 0.4° rotation per projection, 5 frames averaged per projection, and 885 ms exposure time. The scanned images were reconstructed using the same voxel size. The bone-implant interface region up to 300 μm from the implant surface were isolated using imaging software (Image J, NIH) to show 3D image of the regenerated bone tissues surrounding the experimental implant (Fig. 2G).

2.5. Histologic examination and histomorphometric analysis

The undecalcified bone-implant constructs in resin were

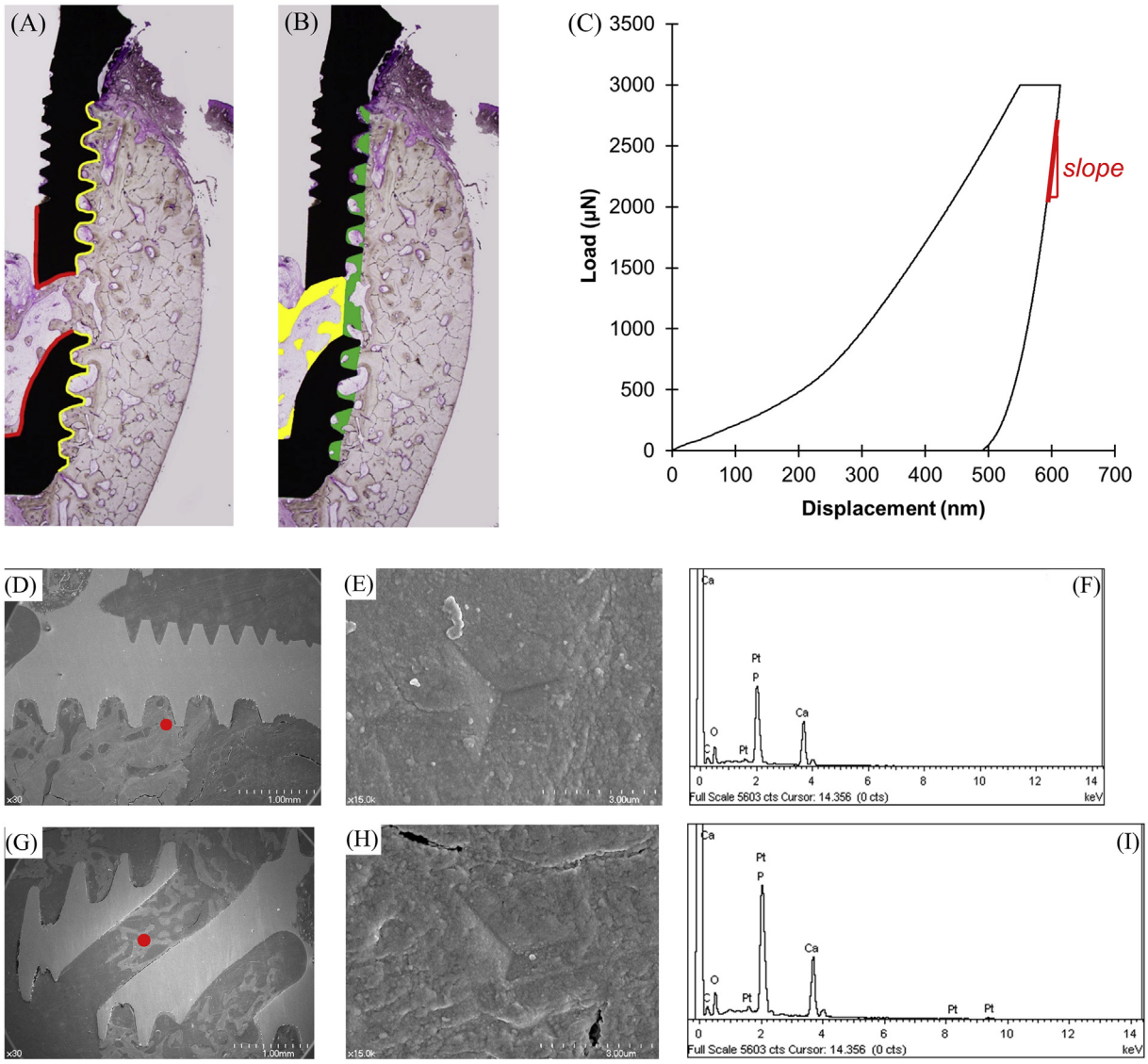

Fig. 3. Schematic drawing of the measurement regions for the histomorphometric analysis. Regions to measure (A) bone-to-implant contact (BIC) and (B) bone-implant interfacial area (BA) indicated by yellow line: total length of implant surface, red line: total length of the side openings and the hollow inner channel, green area: newly formed bone area adjacent to threads (Thread), yellow area: newly formed bone area at the side openings and the hollow inner channel (Ingrowth). (C) Slope of load-displacement curve of nanoindentation used to obtain the reduced modulus (E_r). Scanning electron microscopic (SEM) images of (D) bone-implant interface adjacent outside threads, (G) inside the side opening of the same experimental implant system, and (E) (H) the pyramidal shapes at the indented bone tissue (red dot in (D) and (G)). (F) (I) The energy dispersive spectroscopy (EDS) analysis on the SEM image of the nanoindentation site. The high intensities of calcium (Ca) and phosphorus (P) indicate the newly mineralizing bone tissues next to the metal surface of implant. The peaks for platinum (Pt) arise from the coating process on the specimen surface.

longitudinally dissected in the buccal-lingual direction, ground, and polished to a final thickness less than 50 μm using a cutting and grinding system (EXAKT Apparatebau, Norderstedt, Germany). All processes were conducted with water irrigation. The dissected samples were stained with a multiple stain solution (Polyscience, USA) (Fig. 2). For both control and experimental implant groups, bone-to-implant contact (BIC, mm) was measured along the implant thread line (Fig. 3A, yellow line), and bone-implant interfacial area (BA, mm^2) was defined as an area under a thread apex to next thread apex line within the implant threads (Fig. 3B, green area). For the experimental implant group, the BICs and BAs at the side openings and inner channels below bottom of the abutment screw were also quantified along the inside surface lines of implant (Fig. 3A, red line) and as bone tissues inside the implant (Fig. 3B, yellow area), respectively. The percentage of BIC (BIC (%)) was obtained by computing the ratio of BIC to total length of thread line and that of BA (BA (%)) was determined using the ratio of BA to total area within the threads. The BIC (%) and BA (%) for bone ingrowth into the side openings and hollow inner channels were assessed using ratios of the BIC to total length of surface lines, and the BA to total area below bottom of the abutment screw, respectively.

2.6. Nanoindentation

The sectioned specimens other than used for the histology were subjected to nanoindentation after they were further polished with 1 μm diamond paste using a low speed polisher (Buehler, Lake Bluff, IL). A total of 12 bone-implant constructs including 3 specimens for each control and experimental groups at 3 and 6 weeks after implantation was successfully identified for nanoindentation.

Elastic modulus (E) values of bone tissues at the peri-implant and ingrowth into the implant were measured by probing a pyramidal Berkovich diamond tip of nanoindenter (Ubi-1, Hysitron, Minneapolis,

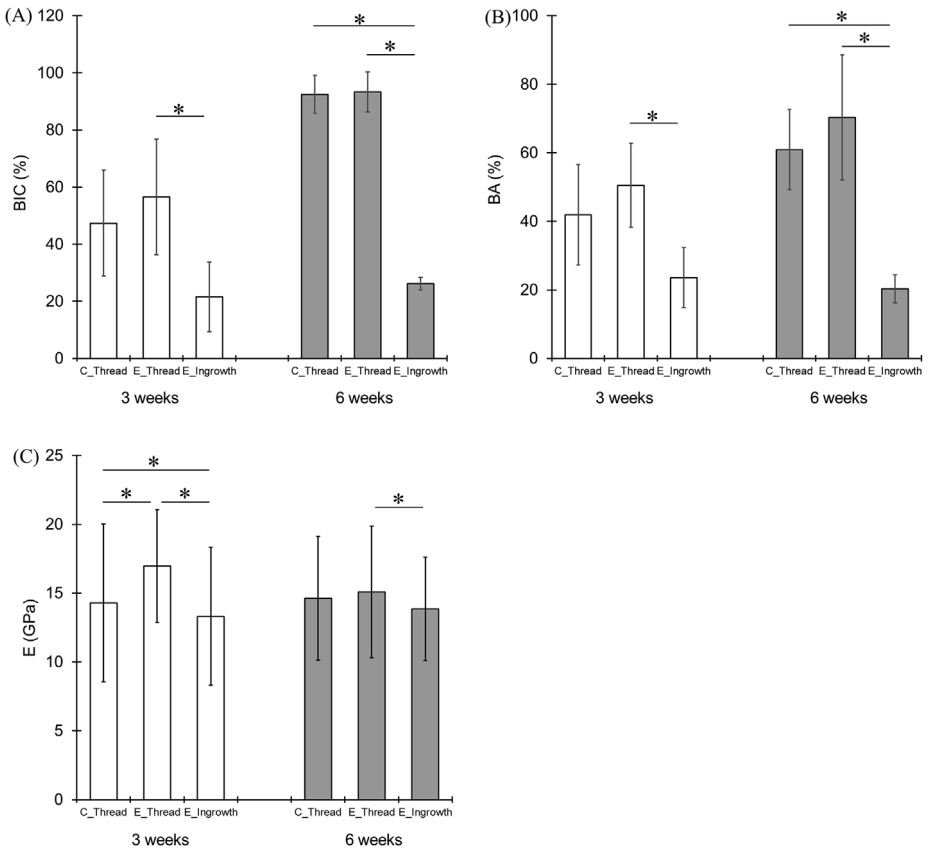

Fig. 4. Comparisons of (A) the percentages of bone-to-implant contact (BIC(%)), (B)bone-implant interfacial area (BA (%)), and (C) nanoindentation elastic modulus (E) values between regions at week 3 and 6. *; $p < 0.031$.

MN). As the nanoindenter was operated by load-control at a load rate of 300 μN/s up to a peak load of 3000 μN. The range of probing depth corresponding to the peak load was at 524.25 ± 108.7 nm. At the process of unloading after the 30-s holding period, the nanoindentation elastic modulus (E) was measured using Eq. (1)(Oliver and Pharr, 2004).

$$\frac{1}{E_r} = \frac{(1-\nu_s^2)}{E_s} + \frac{(1-\nu_i^2)}{E_i} \quad (1)$$

where E_r (reduced modulus) is derived from the slope of the force-displacement curve. E_s is the elastic modulus (E) of the specimen, and ν represents Poisson's ratio. For the diamond indenter, values of $E_i = 1141$ GPa and $\nu_i = 0.07$ are typically used. Poisson's ratio for bone was assigned to be 0.3.

Indentations were performed at the interfacial bone tissue adjacent to the implant thread (Thread) (green area (BA) in Fig. 3B) and pre-existing bone tissue away (> 300 μm) from the implant (Pre-existing) for both control and experimental groups. For the experimental group, additional indentations were conducted for new bone tissues re-generated into the side openings and hollow inner channels below bottom of the abutment screw (Ingrowth) (yellow area (BA) in Fig. 3B). Indentation regions were determined by comparing images of the bone-implant construct, which were taken using a light microscope built in the nanoindenter and a fluorescent microscope to identify the newly formed bone tissues during post-implantation healing periods (Fig. 2CFJM).

2.7. Field emission scanning electron microscopy (FE-SEM)

For further validation, imaging was performed on a FE-SEM (S-4700, HITACHI, Tokyo, Japan) equipped with an energy dispersive x-ray spectrometer (EDX) (EMAX H7200, HORIBA Kyoto, Japan). The specimens were polished and sputter-coated with platinum for 120 s. The operating condition of the FE-SEM was set at 10 kV electron beam energy. The digital image processing and analysis was conducted at the nanoindentation sites (Fig. 3D~I).

2.8. Statistical analysis

The current study obtained 12 control and 12 experimental implant constructs (3 control and 3 experimental dental implants for each animal) from 2 animals at each 3 and 6 weeks of post-implantation healing periods. A total of 23 slices (5 for control and 6 for experimental implant groups at week 3, and 6 for control and 6 for experimental implant groups at week 6) were used for histological analyses. A total of 12 slices (3 for control and 3 for experimental implant groups at week 3 and 6) were used for nanoindentation. The values from measurement errors in the process of searching for indentation surface and statistical outliers were removed as indicated in the previous studies (Hoffler et al., 2000; Kim et al., 2010). Thus, the nanoindentation data obtained from a total number of 3552 indents (748 Thread and 651 Pre-existing regions of the control group and 704 Ingrowth, 783 Thread, and 666 Pre-existing regions of the experimental group) were included for the current analysis. Two way analysis of variance followed by the Tukey-Kramer Post hoc testing for each dependent variable (BIC (%), BA (%), and E) was performed with the post-implantation periods (3 and 6 weeks), and corresponding regions (Ingrowth, Thread, and Pre-existing) included in each implant group (control and experimental) as independent variables. Statistical significance was set at $p < 0.05$.

3. Results

All implantations were successfully completed and no complications were observed during post-implantation healing periods. Newly formed

Table 1
Comparisons of percentages of BIC (%) and BA (%), and elastic modulus (E) for corresponding regions included in control and experimental implant groups (C_Thread control and experimental) between post-implantation periods (3 and 6 weeks). Data are presented as mean ± standard deviation for each parameter.

	C_Thread		E_Thread		E_Ingrowth	
Weeks	3	6	3	6	3	6
BIC (%)	47.381 ± 18.581	92.497 ± 6.655	56.552 ± 20.196	93.382 ± 6.979	21.585 ± 12.235	26.166 ± 2.251
	$p < 0.001$		$p < 0.002$		$p = 0.489$	
BA (%)	41.962 ± 14.631	60.967 ± 11.744	50.506 ± 12.229	70.311 ± 18.259	23.590 ± 8.741	20.287 ± 4.094
	$p = 0.052$		$p = 0.052$		$p = 0.437$	
E (GPa)	14.289 ± 5.738	14.623 ± 4.491	16.964 ± 4.104	15.082 ± 4.773	13.316 ± 5.008	13.864 ± 3.756
	$p = 0.380$		$p < 0.001$		$p = 0.158$	

bone tissues were observed at the bone-implant interfaces of both groups at 3 and 6 weeks of post-implantation healing periods (Fig. 2). In particular, for the experimental implant group, new bone successfully regenerated into the side openings and inner hollow channels, which resulted in bridges between alveolar bones surrounding the implant. The fluorescent microscopic images clearly showed red-labelled new bone tissues adjacent to the implant threads at 3 weeks, and combination of red- and green-labelled bone tissues at 6 weeks of post-implantation healing periods. For the experimental group, the newly formed bone tissues at the side opening and inner channels were also labelled similar to those at the thread regions.

The BIC (%) and BA (%) values at thread regions were not significantly different between control (C_Thread) and experimental (E_Thread) groups at week 3 and 6 ($p > 0.433$) (Figs. 3 and 4A,B) while they increased from week 3 to week 6 ($p < 0.053$) (Table 1). The ingrowth (E_Ingrowth) region had significantly lower BIC (%) and BA (%) values than the thread (E_Thread) region of the experimental group at week 3 and 6 ($p < 0.027$) while they were not significantly different between week 3 and 6 ($p > 0.437$). The values of BIC (%) and BA (%) were not significantly different between C_Thread and E_Ingrowth at week 3 ($p > 0.126$) but the E_Ingrowth region had significantly lower value than thread regions at week 6 ($p < 0.001$).

The Pre-existing region (18.925 ± 4.622 GPa) had significantly higher elastic modulus (E) values than other regions independent of implant groups and post-implantation periods ($p < 0.001$). The E values of E_Thread region were significantly greater than those C_Thread region ($p < 0.001$) while those of E_Ingrowth region were significantly lower values than those of both thread regions at week 3 ($p < 0.031$) (Fig. 4C). The E_Ingrowth region had a significantly lower value of E than the E_Thread region ($p = 0.003$) while it was not significantly different from C_Thread at week 6 ($p = 0.099$). High intensities of calcium (Ca) and phosphorus (P), which are the major components of bone mineral, were detectedat the nanoindentation sites as early as 3 weeks post-implantation (Fig. 3F,I). The atomic % ratios of Ca/P for E_Thread, E_Ingrowth, and Pre-existing regions were 1.42(20.27/14.42), 1.37(19.13/13.97), and 1.65(30.12/18.2), respectively.

4. Discussion

The new hybrid dental implant has been designed to combine threads with the spiral side openings and hollow inner channel, which conduct bone ingrowth into the implant. The side openings are simply perforated onto the threads at the middle portion of conventional screw type dental implant. As such, this design concept can be readily applied to any implant. The threads at the upper portion contacting dense periosteal bone region can provide primary stability of the hybrid implant system comparable with the conventional implant system at the early loading condition. Bone ingrowth into the inner space of the hybrid implant is expected to augment the primary stability with more bone contacts at the implant surface during the long-term loading condition. Also, the threads at the middle and lower portion with closed bottom are designed to provide excellent mechanical strength of the implant and improve its load bearing ability while enhancing bone-implant contacts. Thus, these new architectural components likely overcome the potential risk due to less stability of the previous hollow dental implant that consists of the cylindrical hollow bucket with open bottom floor. Although the upper thread portion was fabricated 3.5 mm in the current animal study, it is recommended to have longer than 4 mm to avoid worst case of marginal bone loss up to 3 mm (Kim, 2017; Standardization, 2007). In addition, as the hollow inner channel is connected to the top opening as well as the side openings, local delivery of medicine is available to stimulate bone regeneration into the open space. The current study focused on validating that this innovative hybrid structure is feasible to provide integration of the implant body with bone tissues grown inside and on the surface of the implant.

New bone tissue apposition continuously increased at the thread regions with longer post-implantation healing as visualized by fluorescent labels (Fig. 2). The interfacial bone next to the threads is damaged by the vigorous implantation surgery (Bosshardt et al., 2017; Insua et al., 2017). Active bone turnover is triggered by bone remodeling to replace the damaged bone with primary bone and then matured secondary osteonal bone. The post-implantation bone resorption lasts about 2 weeks in animal model (Berglundh et al., 2003; Bosshardt et al., 2017). The duration of a single bone remodeling cycle including activation and resorption followed by formation was estimated 12 weeks for dog (Garetto et al., 1995). These observations indicate that continuous apposition of new bone tissues at the thread regions increased new bone-implant contacts and areas up to 6 weeks of post-implantation healing periods in the current study.

The most dramatic finding of the current study is that new bone tissues regenerated through the side openings and bridged across the hollow inner channel as early as 3 weeks of post-implantation healing (Fig. 2). The trabecular shape bone tissue at the side openings and inner channel looks distance osteogenesis, which grows from the resident interfacial bone surrounding the implant. While the new bone tissues were observed in the inner space early at week 3, the bone-implant contacts and areas were not significantly increased but maintained by week 6. It was suggested that large surface area of trabecular bone is more accessible for bone cells to enhance bone turnover (Seeman, 2013; Allen et al., 2011). Similar to the trabecular architecture, the inner open spaces of the hybrid implant may effectively facilitate vascularization providing oxygen and metabolites to promote recruitments of bone cells to accelerate rapid bone turnover without changing the amount of bone. Further long-term studies are needed to find whether angiogenesis involves in the new bone regeneration and the open inner spaces can eventually be fully filled with bone.

The significantly lower nanoindentation elastic modulus (E) values of the interfacial bone tissues than those of the pre-existing indicate that the newly formed interfacial bone tissues have less mineral contents. The more active bone remodeling of the new bone tissue regenerated into the inner open space likely gives rise to the less mineralized bone tissues with the lower value of E. It was indicated that trabecular bone maturation at the implant interface can be observed after 8 weeks of post-implantation (Bosshardt et al., 2017). However, the current study observed that these newly formed bone tissues were as strong as normal bone tissues with the comparable E values higher than 5 GPa independent of post-implantation healing periods. A noticeable finding is that the E value at the thread region of the hybrid implant was significantly higher than at the thread region of the control implant for 3 weeks of post-implantation healing (Fig. 4C). This result suggests that the open spaces also helped accelerate mineralization of the newly forming interfacial bone tissues adjacent to the side openings at the early stage of osseointegration.

The atomic % ratios of Ca/P for E_Thread and E_Ingrowth were much lower than Pre-existing regions. This result is consistent with the

significantly lower nanoindentatin E values measured at the thread and ingrowth regions than the pre-existing region. We suggested that the active bone turnover at the bone-implant interface produces the newly forming less mature bone tissues resulting in the lower mechanical properties for the interfacial bone than the pre-existing bone away from the implant with different treatments and post-implantation healing periods (Kim et al., 2016b) and guided bone regeneration (Johnson et al., 2018) independent of buccal and lingual regions (Kim et al., 2016a). It was also observed that interfacial bone tissues in a porous implant had the less mature characteristics (Shah et al., 2016, 2019). The porous Ti6Al4V implant was fabricated using 3D printing with electron beam melting (EBM) technique and placed the implant in distal femoral epiphyses of sheep. The interfacial bone tissues adjacent to the smooth surface of the implant and generated inside the porous EBM surface had lower Ca/P atomic % ratios but higher organic contents, osteocyte canaliculi per osteocyte lacuna, and osteocyte density than the native bone tissue. These cutting-edge scanning electron microscopy based observations indicate that the newly formed bone tissues have less aged and not fully mature composition at the bone-implant interface and inside of implant pores. On the other hand, masticatory loading continuously stimulates active bone remodeling at the interfacial bone up to 5 years following post-implantation healing while maintaining mechanical stability of the implant system (Baldassarri et al., 2012; Piattelli et al., 2014). Bone tissues with less mineral but higher organic contents have higher static and dynamic time-dependent viscoelastic properties (Kim et al., 2015, 2016b; Les et al., 2004; Viguet-Carrin et al., 2006). As such, these results provide an insight that the newly formed interfacial bone tissues may have an advantage to absorb and dissipate loading energy on the implant system, which likely plays a significant role in the long-term success of an implant system. Future studies need to validate associations between the compositional and structural changes of the interfacial bone tissues and mechanical stability of the implant system.

Thus, a limitation of the current study was that mechanical stability of the whole implant system was not assessed. It was not directly determined whether the bone ingrowth improves load bearing ability of the hybrid implant compared to the traditional screw-type control implant. Nevertheless, the current findings validated the quantity and quality of bone regeneration into the open inner space as well as bone apposition at the implant interface next to threads, which are critical factors to maintain a stable implant system under masticatory loading. Another limitation is that the current results were obtained without *in vivo* loading on the implant systems. It has been observed that loading could stimulate bone remodeling at the implant interface (Baldassarri et al., 2012) but its effects on bone ingrowth into the inner space of implant have not been investigated. The current study focused only on early healing process following implantation prior to practical loading.

5. Conclusion

The size and architecture of spiral side openings and hollow inner channel at the middle portion of the one-piece hybrid dental implant can conduct bone ingrowth at the early post-implantation healing period. The newly regenerated bone tissue in the inner space had comparable quality with the normal bone tissue. The quantity of new bone apposition at the thread portion of the hybrid implant was similar to that of the conventional screw type implant. The side openings could also improve quality of the newly forming interfacial bone tissue at the early post-implantation healing period. These results strongly support efficacy of the open inner space concept in the new hybrid implant as an effective scaffold to conduct active bone regeneration. Future application can include local drug delivery through the top opening of the hybrid implant to treat peri-implantitis and accelerate bone regeneration at less bone sites, critical size defects, and sinus lifting. With success of these approaches, the current hybrid system can expand the conventional concept of osseointegration.

Conflicts of interest

The authors have no conflict of interests to publication of this study.

Acknowledgements

This research was supported by OSU College of Dentistry seed grant (Kim, DG), and Biomedical Technology Development Program of the National Research Foundation of Korea funded by the Ministry of Science and ICT, Korea (NRF-2014M3A9E3064466).

References

Allen, M.R., Turek, J.J., Phipps, R.J., Burr, D.B., 2011. Greater magnitude of turnover suppression occurs earlier after treatment initiation with risedronate than alendronate. Bone 49, 128–132 doi:S8756-3282(10)01354-2 [pii]10.1016/j.bone.2010.07.011.

Baldassarri, M., Bonfante, E., Suzuki, M., Marin, C., Granato, R., Tovar, N., Coelho, P.G., 2012. Mechanical properties of human bone surrounding plateau root form implants retrieved after 0.3-24 years of function. J. Biomed. Mater. Res. B Appl. Biomater. 100, 2015–2021. https://doi.org/10.1002/jbm.b.32786.

Behneke, A., Behneke, N., d'Hoedt, B., 2002. A 5-year longitudinal study of the clinical effectiveness of ITI solid-screw implants in the treatment of mandibular edentulism. Int. J. Oral Maxillofac. Implant. 17, 799–810.

Berglundh, T., Abrahamsson, I., Lang, N.P., Lindhe, J., 2003. De novo alveolar bone formation adjacent to endosseous implants. Clin. Oral Implant. Res. 14, 251–262.

Bosshardt, D.D., Chappuis, V., Buser, D., 2017. Osseointegration of titanium, titanium alloy and zirconia dental implants: current knowledge and open questions. Periodontol 73, 22–40. https://doi.org/10.1111/prd.12179. 2000.

Branemark, P.I., Hansson, B.O., Adell, R., Breine, U., Lindstrom, J., Hallen, O., Ohman, A., 1977. Osseointegrated implants in the treatment of the edentulous jaw. Experience from a 10-year period. Scand. J. Plast. Reconstr. Surg. Suppl. 16, 1–132.

Brunski, J.B., 1988. Biomaterials and biomechanics in dental implant design. Int. J. Oral Maxillofac. Implant. 3, 85–97.

Buser, D., Mericske-Stern, R., Bernard, J.P., Behneke, A., Behneke, N., Hirt, H.P., Belser, U.C., Lang, N.P., 1997. Long-term evaluation of non-submerged ITI implants. Part 1: 8-year life table analysis of a prospective multi-center study with 2359 implants. Clin. Oral Implant. Res. 8, 161–172.

Charyeva, O., Altynbekov, K., Zhartybaev, R., Sabdanaliev, A., 2012. Long-term dental implant success and survival–a clinical study after an observation period up to 6 years. Swed. Dent. J. 36, 1–6.

Garetto, L.P., Chen, J., Parr, J.A., Roberts, W.E., 1995. Remodeling dynamics of bone supporting rigidly fixed titanium implants: a histomorphometric comparison in four species including humans. Implant Dent. 4, 235–243.

Greenstein, G., Cavallaro, J., 2014. Failed dental implants: diagnosis, removal and survival of reimplantations. J. Am. Dent. Assoc. 145, 835–842. https://doi.org/10.14219/jada.2014.28.

Hellem, S., Karlsson, U., Almfeldt, I., Brunell, G., Hamp, S.E., Astrand, P., 2001. Nonsubmerged implants in the treatment of the edentulous lower jaw: a 5-year prospective longitudinal study of ITI hollow screws. Clin. Implant Dent. Relat. Res. 3, 20–29.

Hoffler, C.E., Moore, K.E., Kozloff, K., Zysset, P.K., Brown, M.B., Goldstein, S.A., 2000. Heterogeneity of bone lamellar-level elastic moduli. Bone 26, 603–609.

Horowitz, R., Holtzclaw, D., Rosen, P.S., 2012. A review on alveolar ridge preservation following tooth extraction. J. Evid. Based Dent. Pract. 12, 149–160. https://doi.org/10.1016/S1532-3382(12)70029-5.

Insua, A., Monje, A., Wang, H.L., Miron, R.J., 2017. Basis of bone metabolism around dental implants during osseointegration and peri-implant bone loss. J. Biomed. Mater. Res. A 105, 2075–2089. https://doi.org/10.1002/jbm.a.36060.

Johnson, T.B., Siderits, B., Nye, S., Jeong, Y.H., Han, S.H., Rhyu, I.C., Han, J.S., Deguchi, T., Beck, F.M., Kim, D.G., 2018. Effect of guided bone regeneration on bone quality surrounding dental implants. J. Biomech. 80, 166–170. https://doi.org/10.1016/j.jbiomech.2018.08.011.

Karoussis, I.K., Bragger, U., Salvi, G.E., Burgin, W., Lang, N.P., 2004. Effect of implant design on survival and success rates of titanium oral implants: a 10-year prospective cohort study of the ITI dental implant system. Clin. Oral Implant. Res. 15, 8–17.

Kim, D.G., Elias, K.L., Jeong, Y.H., Kwon, H.J., Clements, M., Brantley, W.A., Lee, D.J., Han, J.S., 2016a. Differences between buccal and lingual bone quality and quantity of peri-implant regions. J. Mech. Behav. Biomed. Mater. 60, 48–55. https://doi.org/10.1016/j.jmbbm.2015.12.036.

Kim, D.G., 2017. US 9757213B2 In: U. S. P. a. T. Office (Ed.), Hybrid Dental Implant. Ohio State Innovation Foundation, USA.

Kim, D.G., Huja, S.S., Lee, H.R., Tee, B.C., Hueni, S., 2010. Relationships of viscosity with contact hardness and modulus of bone matrix measured by nanoindentation. J. Biomech. Eng. 132, 024502. https://doi.org/10.1115/1.4000936.

Kim, D.G., Jeong, Y.H., Kosel, E., Agnew, A.M., McComb, D.W., Bodnyk, K., Hart, R.T., Kim, M.K., Han, S.Y., Johnston, W.M., 2015. Regional variation of bone tissue properties at the human mandibular condyle. Bone 77, 98–106. https://doi.org/10.1016/j.bone.2015.04.024.

Kim, D.G., Kwon, H.J., Jeong, Y.H., Kosel, E., Lee, D.J., Han, J.S., Kim, H.L., Kim, D.J., 2016b. Mechanical properties of bone tissues surrounding dental implant systems with different treatments and healing periods. Clin. Oral Investig. 20, 2211–2220.

https://doi.org/10.1007/s00784-016-1734-2.
Les, C.M., Spence, C.A., Vance, J.L., Christopherson, G.T., Patel, B., Turner, A.S., Divine, G.W., Fyhrie, D.P., 2004. Determinants of ovine compact bone viscoelastic properties: effects of architecture, mineralization, and remodeling. Bone 35, 729–738. https://doi.org/10.1016/j.bone.2004.04.006.
Oliver, W.C., Pharr, G.M., 2004. Measurement of hardness and elastic modulus by instrumented indentation: advances in understanding and refinements to methodology. J. Mater. Res. 19, 3–20. https://doi.org/10.1557/jmr.2004.19.1.3.
Piattelli, A., Artese, L., Penitente, E., Iaculli, F., Degidi, M., Mangano, C., Shibli, J.A., Coelho, P.G., Perrotti, V., Iezzi, G., 2014. Osteocyte density in the peri-implant bone of implants retrieved after different time periods (4 weeks to 27 years). J. Biomed. Mater. Res. B Appl. Biomater. 102, 239–243. https://doi.org/10.1002/jbm.b.33000.
Piattelli, A., Scarano, A., Piattelli, M., Vaia, E., Matarasso, S., 1999. A microscopical evaluation of 24 retrieved failed hollow implants. Biomaterials 20, 485–489. https://doi.org/10.1016/S0142-9612(98)00194-X.
Pjetursson, B.E., Asgeirsson, A.G., Zwahlen, M., Sailer, I., 2014. Improvements in implant dentistry over the last decade: comparison of survival and complication rates in older and newer publications. Int. J. Oral Maxillofac. Implant. 29 (Suppl. l), 308–324. https://doi.org/10.11607/jomi.2014suppl.g5.2.
Scacchi, M., 2000. The development of the ITI DENTAL IMPLANT SYSTEM. Part 1: a review of the literature. Clin. Oral Implant. Res. 11 (Suppl. 1), 8–21.
Seeman, E., 2013. Age- and menopause-related bone loss compromise cortical and trabecular microstructure. J. Gerontol. A Biol. Sci. Med. Sci. 68, 1218–1225. https://doi.org/10.1093/gerona/glt071.
Shah, F.A., Ruscsak, K., Palmquist, A., 2019. 50 years of scanning electron microscopy of bone-a comprehensive overview of the important discoveries made and insights gained into bone material properties in health, disease, and taphonomy. Bone Res. 7. https://doi.org/10.1038/s41413-019-0053-z.
Shah, F.A., Snis, A., Matic, A., Thomsen, P., Palmquist, A., 2016. 3D printed Ti6Al4V implant surface promotes bone maturation and retains a higher density of less aged osteocytes at the bone-implant interface. Acta Biomater. 30, 357–367. https://doi.org/10.1016/j.actbio.2015.11.013.
Standardization, I.O.f., 2007. Dynamic Fatigue Test for Endosseous Dental Implants. ISO 14801:2007.
Takeshita, F., Suetsugu, T., Higuchi, Y., Oishi, M., 1996. Histologic study of failed hollow implants. Int. J. Oral Maxillofac. Implant. 11, 245–250.
Taniguchi, N., Fujibayashi, S., Takemoto, M., Sasaki, K., Otsuki, B., Nakamura, T., Matsushita, T., Kokubo, T., Matsuda, S., 2016. Effect of pore size on bone ingrowth into porous titanium implants fabricated by additive manufacturing: an in vivo experiment. Mater. Sci. Eng. C Mater. Biol. Appl. 59, 690–701. https://doi.org/10.1016/j.msec.2015.10.069.
Telleman, G., Meijer, H.J., Raghoebar, G.M., 2006. Long-term evaluation of hollow screw and hollow cylinder dental implants: clinical and radiographic results after 10 years. J. Periodontol. 77, 203–210. https://doi.org/10.1902/jop.2006.040346.
Tonetti, M.S., Hammerle, C.H., European Workshop on Periodontology Group C, 2008. Advances in bone augmentation to enable dental implant placement: consensus report of the sixth European workshop on periodontology. J. Clin. Periodontol. 35, 168–172. https://doi.org/10.1111/j.1600-051X.2008.01268.x.
Viguet-Carrin, S., Garnero, P., Delmas, P.D., 2006. The role of collagen in bone strength. Osteoporos. Int. 17, 319–336. https://doi.org/10.1007/s00198-005-2035-9.
Wang, R.E., Lang, N.P., 2012. Ridge preservation after tooth extraction. Clin. Oral Implant. Res. 23 (Suppl. 6), 147–156. https://doi.org/10.1111/j.1600-0501.2012.02560.x.
Wang, Z.H., Wang, C.Y., Li, C., Qin, Y.G., Zhong, L., Chen, B.P., Li, Z.Y., Liu, H., Chang, F., Wang, J.C., 2017. Analysis of factors influencing bone ingrowth into three-dimensional printed porous metal scaffolds: a review. J. Alloy. Comp. 717, 271–285. https://doi.org/10.1016/j.jallcom.2017.05.079.